Magnesium atoms in an intense nonresonant laser field

Dalwoo Kim,* S. Fournier,† M. Saeed,‡ and L. F. DiMauro
Department of Chemistry, Brookhaven National Laboratory and Associated Universities, Upton, New York 11973
(Received 21 November 1989)

A spectroscopic study on the nonresonant multiphoton ionization of magnesium atoms in a high-intensity laser field is reported. Both 0.532- and 1.06-μm radiation in the intensity regime of 10^{10}–10^{13} W/cm^2 are used to produce both singly and doubly ionized magnesium ions. Mass and angularly resolved electron-energy analyses were used in an attempt to gain insight into the dominant mechanisms responsible for ionization. An analysis is presented for intensity- and frequency-dependent results, and electron angular distributions are reduced in terms of atomic parameters derivable from lowest-order perturbation theory. The results demonstrate the important influence that the details of the atomic structure have in describing the high-field nonresonant ionization of magnesium.

I. INTRODUCTION

When an atom interacts with a nonresonant high-intensity laser field, it can absorb one or more photons, which results in some degree of ionization. In the limit where the photon energy is much less than the binding energy of the atom, highly nonlinear absorption results in the observation of many dramatic effects, i.e., above-threshold ionization (ATI)[1–3] and high-harmonic generation.[4] These experiments, among others, have long established the important influence that the electromagnetic field (via the ponderomotive potential) has upon the spectroscopy, as well as the dynamics of these processes. However, the extent to which the atomic structure plays a role at these high intensities remains an open question. A Keldysh-Faisal-Reiss (KFR) model,[5,6] which incorporates a minimal description of an atom's structure, has been successful in describing some aspects of the ATI spectrum of inert gases. Perry *et al.* have used an extended KFR model,[7] which accounts for the Coulomb field in the final state; their calculations have resulted in excellent agreement with intensity-dependent data from inert-gas ion-yield curves. Some very recent experiments on xenon atoms by Freeman *et al.*[8] and Muller *et al.*[9] have unmasked the important influence of the atomic structure in the subpicosecond pulse regime. They found that bound states, i.e., Rydberg series, of the atom shift into resonance via the ponderomotive shift and are exhibited as peaks in the photoelectron spectrum. Tang, Lyras, and Lambropoulos[10] have presented a theoretical analysis that describes these experiments using a density-matrix formalism that is allowed to evolve in a realistic temporal and spatial pulse shape. Clearly, an analytical description of ionization for any atom in the short pulse limit must include some aspects of the atomic structure.

A number of studies,[11–13] including our previous work on calcium,[14] have focused on determining the role of doubly excited states in the multiphoton ionization (MPI) of alkaline-earth atoms. These studies emphasize not only the essential role of the atomic structure but also the importance of electron correlations. In this paper we report on the nonresonant ionization of magnesium atoms with 1.06- and 0.532-μm radiation in the intensity regime of $I < 10^{13}$ W/cm^2. The MPI of alkaline-earth atoms poses an interesting alternative to that of rare-gas atoms in that their atomic structure near threshold contains manifolds of doubly excited states. Also, the low-Z alkaline-earth atoms provide an opportunity for a more complete theoretical description. Specifically, magnesium is a necessary atom to study within the alkaline-earth group if a complete physical picture is to be achieved. As was pointed out by Greene,[15] the alkaline-earth atoms, which all have an ns^2 ground-state designation, can be characterized into two distinct groups within a single-photon description. The two groups illustrate differing degrees of manifestations of electron correlations in the discrete energy region. Accordingly, the spectra of Be and Mg are similar, but are qualitatively different from the spectra of the higher-Z alkaline earth elements, which are similar among themselves. In this regard it would be interesting to contrast the earlier MPI work on high-Z alkaline earth atoms to the current results on magnesium.

II. EXPERIMENT

A detailed description of the experimental apparatus and analysis procedure is given in our earlier work.[14] Briefly, neutral magnesium atoms continuously produced by an effusive oven are ionized by 10-ns pulses from a well-diagnosed Nd:YAG laser. The laser and atomic beam intersect at right angles in a high-vacuum chamber. The electrons or ions produced in the process are analyzed by a time-of-flight spectrometer. The arrival times are detected by microchannel plate detectors, processed by a transient recorder, and subsequently stored to a PDP11/73 computer. The data are analyzed for electron energies and spatial anisotropy, intensity dependence, and ion distributions. The laser is operated at a constant power output and the energy and polarization are externally varied. For the intensity studies the laser polariza-

tion is fixed parallel to the spectrometer's axis. The experimental system is well characterized to minimize the effects of space charge and contact potentials. The data at all wavelengths was evaluated such that the total number of ions produced in the interaction volume resulted in no detectable space-charge distortions of our results. This corresponded to a maximum total ion yield per laser shot of 50–100.

III. RESULTS AND DISCUSSION

A. Electron-energy spectrum

Figure 1 shows the relevant energy levels for magnesium along with several electron decay channels resulting from 532-nm excitation. The ionization threshold value for singly and doubly ionized magnesium are 7.64 and 15.04 eV, respectively. The lowest-order ionization process for neutral ground-state magnesium with 532-nm radiation is

$$\mathrm{Mg}(3s^2)+4h\nu\rightarrow\mathrm{Mg}^+(3s)+e(1.68\ \mathrm{eV})\ . \quad (1)$$

Sequential ionization of the Mg^+ ground state yields

$$\mathrm{Mg}^+(3s)+7h\nu\rightarrow\mathrm{Mg}^{2+}(2p^6)+e(1.28\ \mathrm{eV})\ . \quad (2)$$

In each instance, an electron is created with a discrete energy that is given in parentheses. Conversely, ionization of neutral magnesium can result in direct two-electron ejection via

$$\mathrm{Mg}(3s^2)+10h\nu\rightarrow\mathrm{Mg}^{2+}(2p^6)+2e(\text{continuous})\ . \quad (3)$$

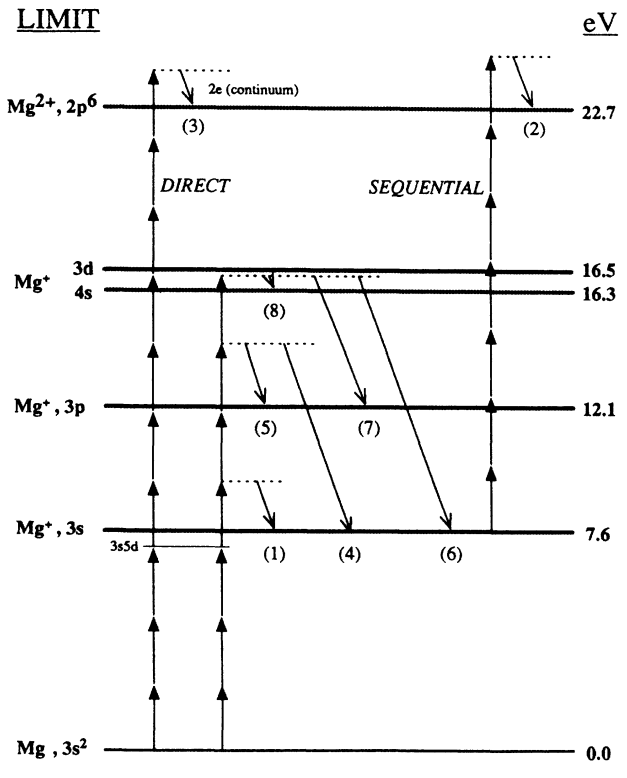

FIG. 1. Energy-level diagram for magnesium showing threshold levels relevant to this study. The numbers in parentheses correlate with the equation numbers in the text and the excitation is illustrated for 532-nm photons. The energies are referenced with respect to the neutral magnesium ground state.

The consequence of this process is a highly correlated electron motion resulting in a continuous electron spectrum that is quite distinct from the discrete sequential electrons. This continuous spectrum arises since all combinations for sharing the excess energy between the two electrons are equally probable. Although the spectral feature of direct ionization is distinctive, practical experimental limitations at these high intensities make detection difficult. A number of groups[11,12,14,16] have looked for explicit evidence for direct ionization with no satisfactory result.

Similar to the case of calcium,[14] the absorption of two or more additional 532-nm photons can result in a physical picture that can be quite different from "single electron" ATI as observed in rare gases. This is a consequence of new decay channels that energetically open just above the first ionization limit, specifically, the $3p$ and $4s$ thresholds open at the six- and seven-photon level, respectively. The resulting electron-energy spectrum would be as follows:

$$\mathrm{Mg}(3s^2)+(4+2)h\nu\begin{cases}\rightarrow\mathrm{Mg}^+(3s)+e(6.35\ \mathrm{eV})\ \mathrm{ATI}\\ \quad\text{for } 1.68\ \mathrm{eV} \quad (4)\\ \rightarrow\mathrm{Mg}^+(3p)+e(1.91\ \mathrm{eV}) \quad (5)\end{cases}$$

$$\mathrm{Mg}(3s^2)+(4+3)h\nu\begin{cases}\rightarrow\mathrm{Mg}^+(3s)+e(8.68\ \mathrm{eV})\ \mathrm{ATI}\\ \quad\text{for } 1.68\ \mathrm{eV} \quad (6)\\ \rightarrow\mathrm{Mg}^+(3p)+e(4.25\ \mathrm{eV})\ \mathrm{ATI}\\ \quad\text{for } 1.91\ \mathrm{eV} \quad (7)\\ \rightarrow\mathrm{Mg}^+(4s)+e(0.01\ \mathrm{eV})\ . \quad (8)\end{cases}$$

Processes (4) and (6) are synonymous to the ATI spectrum observed in inert gases.[2] However, paths (5), (7), and (8) decay to excited ionic states. Clearly, the final state of the process resulted from the excitation of two electrons, one ionized and one in an excited core. Likewise, paths (4) and (6) would have also evolved with some probability of two-electron excitation or correlation. Thus we see a distinction between ATI in inert gases and alkaline-earth atoms, where one-electron ionization does not necessarily signify a single-electron excitation. Consequently, an independent electron picture could result in an inadequate description of the ionization dynamics of alkaline-earth atoms and a more complete model must incorporate correlation effects.[17] Experimental studies[11,12,14] on high-Z alkaline earth atoms implicate such a description. However, magnesium differs from the higher-Z alkaline earth atoms in that the discrete spectrum shows less mixing with the higher-lying doubly excited channels.

Figure 2 is the electron-energy spectrum of magnesium with 532-nm excitation at an intensity of 2×10^{12} W/cm^2. The spectrum consists of a series of peaks corresponding to the formation of both singly and doubly ionized mag-

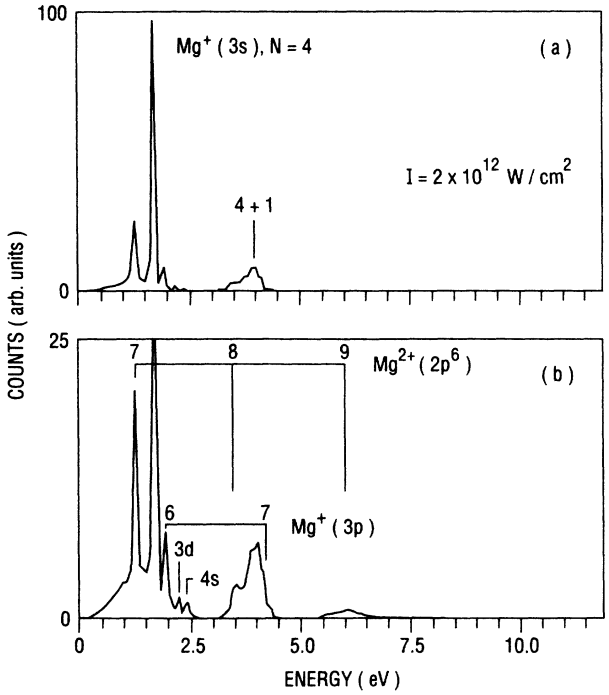

FIG. 2. Electron-energy spectrum of magnesium resulting from 532-nm excitation. (a) The laser intensity is 2×10^{12} W/cm^2 and (b) is a four-times-expanded view.

nesium. The most dominant feature is the four-photon ionization of the $3s^2$ ground state via path (1) and its associated ATI series occurring at 4.01, 6.35, and 8.68 eV. The peak at 1.28 eV corresponds to the seven-photon sequential ionization of the $3s$ ground state of Mg^+ via path (2). The appearance of this peak correlated well with the detection of Mg^{2+} in our mass spectrometer. However, any quantitative mass analysis of the doubly ionized Mg was hindered by a persistent carbon ion peak, whose m/q ratio is degenerate with that of Mg^{2+}. No clear evidence exists within our detection limit for the formation of Mg^{2+} by direct ionization. Consequently, as was the case with calcium,[14] the results show that sequential ionization is the predominant mechanism for the formation of doubly charged ions with 10-ns laser pulses. This conclusion does not presume that the transition dynamics is restricted to an independent electron description. In fact, closer examination of Fig. 2(b) reveals the presence of a number of weaker peaks which can be assigned to excited Mg^+ ions. The peak at 1.91 eV corresponds to a six-photon absorption decaying to the $3p\ ^2P$ excited state of the Mg^+ ion along with its ATI peak at 4.25 eV. The weak doublet peaks at 2.13 and 2.34 eV are tentatively assigned to the eight-photon absorption leaving the ion in excited $3d$ and $4s$ states, respectively. The peak at 2.34 eV is the first ATI peak above the $4s$ threshold; the corresponding lowest-order peak above this threshold [path (8)] has a near-zero kinetic energy, making it difficult to detect with our apparatus. Furthermore, at the saturation intensity the shift (mostly ponderomotive) in the ionization potential could be significant in suppressing and scattering this channel. Although it is difficult to give an absolute measure of the branching ratio at a specific total photon energy, some general comments can be made. Paths (4) and (5) both correspond to six-photon ionization with the latter resulting in an excited $3p$ state ion. A lower-limit branching percentage of $3p$ to $3s$ is 60% to 40%. It is interesting to compare this result with the 76–80 % branching to the $3p$ ionic state predicted for the one-photon ionization using an eigenchannel R-matrix method.[18] At the eight-photon level, four decay paths exist, the branching ratio to the $4s$ and $3d$ channels appear equal while there is no detectable $3s$ decay, and resolution difficulties make it impossible to deconvolute any branching to the $3p$ channel. Again, these values represent only limits and a more exact result relies upon knowledge of the spatial anisotropy for each channel and the energy transmission characteristics of our spectrometer. However, the results do demonstrate that two-electron or double excitation is occurring and competing significantly with single-electron excitation.

Figure 3 shows electron-energy spectra of magnesium resulting from 1.06-μm excitation at intensities below and above saturation. The strong peak at 0.51 eV is assigned to the seven-photon ionization resulting in the formation of a ground-state Mg^+ ion. The peaks at 1.68, 2.84, 4.00,

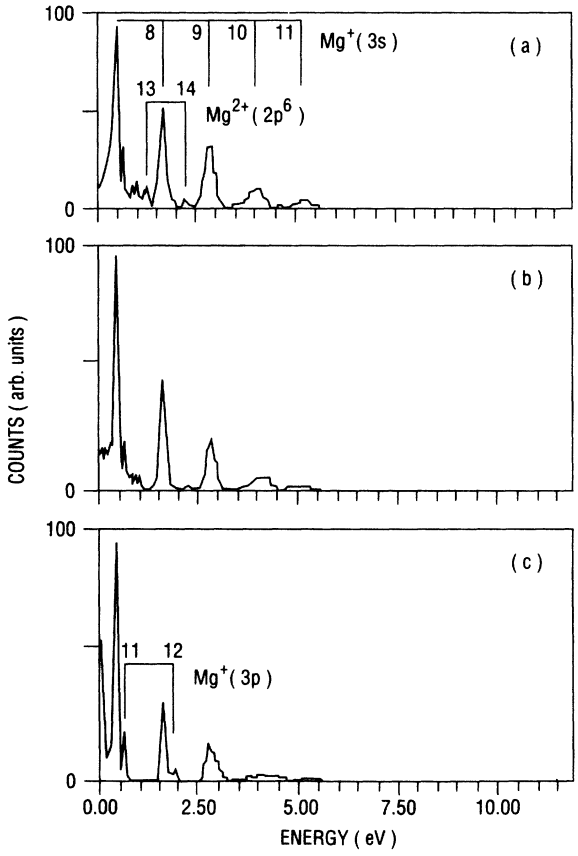

FIG. 3. Electron-energy spectrum of magnesium resulting from 1.06-μm excitation: (a) $I=5.0\times10^{12}$ W/cm^2, (b) $I=1.0\times10^{12}$ W/cm^2, and (c) $I=5.0\times10^{11}$ W/cm^2.

and 6.33 eV are the associated ATI series resulting from absorption of up to four additional photons. An obvious outcome of increasing the order of nonlinearity for a nonresonant process results in a higher saturation intensity and, consequently, a more prevalent ATI series as compared with the 532-nm excitation spectrum of Fig. 2. Also identified are peaks at 1.28 and 2.44 eV, which are assigned to the ATI series resulting from sequential ionization via

$$Mg^+(3s)+(13+S)h\nu \rightarrow Mg^{2+}(2p^6)+e \ , \tag{9}$$

where $S=1$ and 2, respectively. The magnitude of the ponderomotive potential under these conditions is significant and presumably contributes to the absence of the 0.1-eV electron associated with the lowest-order 13-photon absorption. Again, the main focus of attention in Fig. 3 is the peaks corresponding to the production of excited-state Mg^+ ions. The $3p$ excited-state series have been well identified in our spectra,

$$Mg(4s^2)+(11+S)h\nu \rightarrow Mg^+(3p)+e(\varepsilon) \ , \tag{10}$$

where $S=0$, 1, and 2 and ε equals 0.75, 1.91, and 3.08 eV, respectively. Electron peaks observed at 0.97 and 1.17 eV are tentatively identified as the 15-photon absorption above the $3d$ and $4s$ thresholds, respectively. These peaks are only observed at high intensities but are reproducible. They are not associated with background ionization or the purity of the magnesium sample. Likewise, the lowest-order peak decaying to the $4s$ final state is not observed but this would be consistent with the arguments given above, especially as they applied to the ponderomotive shift of the ionization potential at saturation.

An initial inspection of Figs. 2 and 3 would suggest that the production of excited states is less significant at 1.06-μm as compared to 532-nm excitation. This is understood by considering that the number of additional photons necessary to reach the excited-state channels is larger for 1.06-μm than with 532 nm. However, if one alternatively views the decay branching at some fixed photon energy above any of the excited channels, we see that excited-state formation is comparable to that at 532 nm. This result is surprising since, in the discrete spectrum at the six-photon absorption energy, an electric-dipole-allowed $3s5d\ ^1D$ bound state is detuned only 80 cm^{-1} to the red. If such a state is dominating the transition dynamics, one would expect a scenario best described by an independent electron model. However, the experimental evidence with 1.06-μm excitation shows that two-electron excitation is still having a significant influence on the overall transition dynamics.

B. Intensity effects

Lowest-order perturbation theory predicts that for an N-photon nonresonant process the number of counts should increase as I^N. Similarly, the saturation flux F_S, which is defined as the fluence necessary to ionize all atoms with unit probability within the laser field, can be expressed as[19]

$$F_S=\Lambda_N^{-1}\tau_{\text{eff}}^{-1/N} \ . \tag{11}$$

τ_{eff} is an effective laser pulse duration and Λ_N is defined as $(\sigma_N)^{1/N}$, where σ_N is the generalized N-photon cross section. The values for Λ_N are estimated for magnesium by scaling the calculated hydrogenic values.[19] The experimental results for the nonlinearity N and the saturation intensity I_S^{expt} for a number of electron channels are summarized in Table I. For these studies, the laser polarization is fixed parallel to the spectrometer's axis. A mass spectrometer was also used to measure the total Mg^+ ion yield but was not applicable to Mg^{2+} detection, as discussed above. These results are also presented in Table I along with saturation intensities I_S^{calc} derived from Eq. (11). The nonlinearity was derived by least-squares analysis of the linear portion of a log-log plot of electron (ion) counts versus laser intensity.

Analysis of the 1.68-eV electron channel [path (1)] and its ATI peak at 4.01 eV resulting from 532-nm excitation yields an intensity dependence consistent with perturbative scaling and saturation intensities that are similar. The analysis based on the total Mg^+ ion yield curves as determined from mass spectroscopy renders excellent agreement with the electron data. The measured slope for the 1.28-eV electron peak is consistent with our assignment based on seven-photon sequential ionization of the Mg^+ ground state via path (2). However, due to our inability to quantitatively measure the total Mg^{2+} ion yield, this analysis can not exclude direct ionization. Although within the detection sensitivity of our electron spectrometer, no evidence exists to support appreciable direct ionization. Likewise, the results listed in Table I for 1.06-μm ionization show similar agreement with perturbative scaling laws. This is further demonstrated by the good agreement between the experimental values and those calculated using Eq. (11) at both laser frequencies. This agreement is certainly expected considering the modest saturation intensities in these experiments. It would be interesting to test whether this is true at shorter pulse durations where the atoms will experience higher intensities. Finally, the analysis of the intensity curves for the 0.51-eV electron associated with the lowest-order ionization of ground-state Mg atoms, as well as the total Mg^+ ion yield, gives a result consistent with seven-photon absorption. This evidence suggests that the above-mentioned $3s5d$ bound state, which is nearly degenerate at the six-photon energy, is not dominating the ionization dynamics. Furthermore, this corroborates our earlier contention concerning the propensity of excited-state formation.

C. Angular distributions

Electron angular distributions provide valuable insight into the atomic transition matrix elements and thus a useful test of theoretical models. However, for multiphoton ionization with high-field strengths, care must be taken to avoid scattering of the *atomic* distributions due to field (ponderomotive)[20,21] and/or space-charge effects.[22] This problem becomes magnified for low-energy electrons and at long wavelengths since the ponderomotive potential scales as ω^{-2}. The angular distributions reported here were carefully evaluated to minimize such effects. The

TABLE I. Order of nonlinearity and saturation intensities for magnesium. Standard deviations are indicated in parentheses. The values for I_S^{calc} are calculated using Eq. (11).

Ionization process	N	I_S^{expt} (GW/cm^2)	I_S^{calc} (GW/cm^2)
	Excitation: 0.532-μm radiation		
$Mg(3s^2)+4h\nu \rightarrow Mg^+(3s)+e(1.68\ eV)$	4.2(5)	320(110)	
$Mg(3s^2)+(4+1)h\nu \rightarrow Mg^+(3s)+e(4.01\ eV)$	5.3(6)	390(110)	
$Mg^+(3s)+7h\nu \rightarrow Mg^{2+}(2p^6)+e(1.28\ eV)$	5.2(15)	2500(900)	5000
Total Mg^+ yield	4.4(4)	280(90)	160
	Excitation: 1.06-μm radiation		
$Mg(3s^2)+7h\nu \rightarrow Mg^+(3s)+e(0.51\ eV)$	6.7(6)	430(140)	
$Mg(3s^2)+(7+1)h\nu \rightarrow Mg^+(3s)+e(1.68\ eV)$	7.8(5)	400(100)	
$Mg(3s^2)+(7+2)h\nu \rightarrow Mg^+(3s)+e(2.84\ eV)$	9.2(8)	370(100)	
$Mg(3s^2)+(7+3)h\nu \rightarrow Mg^+(3s)+e(4.01\ eV)$	9.7(9)	430(110)	
Total Mg^+ yield	6.9(7)	250(150)	300

data were recorded at low atomic beam densities to reduce space-charge effects and, when possible, collected at low intensities, i.e., below saturation. To facilitate the detection of any systematic asymmetries produced in the distributions due to imperfect optics or misalignments, the data were collected over π radians of the electric-field vector.

Information about the atomic matrix elements is obtained from the experimental angular distributions by fitting to the well-known expression for an N-photon nonresonant process given by

$$I(\theta)=\sum_{i=1}^{N}\beta_{2i}P_{2i}(\cos\theta)\ , \tag{12}$$

where $P_{2i}(\cos\theta)$ is the Legendre polynomial of order $2i$, θ is the angle between the electric-field vector and the momentum of the photoelectron, and β_{2i} are the atomic parameters. The experimental β coefficients are directly comparable to those derived by theory and would benefit from such a comparison. In fact, calculations for the lowest-order processes are in progress.[17] The results of the fit to Eq. (12) are listed in Tables II and III and illustrated as solid curves in Figs. 4 and 5. The parameters are normalized with respect to the β_2 coefficient and allowed to fit with the maximum number of $(N+1)$ terms. Analyses of the distributions using higher-order parameters were performed in order to test the integrity of the fits; this resulted in no significant improvement in the statistical variance.

Electron distributions resulting from ionization of Mg and Mg^+ ground-state atoms via 532-nm excitation are shown as open circles in Fig. 4. Distributions (a), (b), and (c) in Fig. 4 are those resulting from the production of $3s$ ground-state Mg^+ ions following the absorption of 4, 5, and 6 photons, respectively. The spatial anisotropy becomes more pronounced along the e-field direction as the number of absorbed photons increases and alternates between local maxima-minima normal to the e-field direction in accordance with the number of absorbed photons. Furthermore, absorption of six 532-nm photons results in a total energy above the $3p$ threshold. Consequently, the branching, as identified in the earlier discussion, results in nearly equal amounts of $3s$ ground- or $3p$ excited-state ion formation. The $3s$ and $3p$ angular distributions are shown in Figs. 4(c) and 4(d), respectively. The two plots are quite different in appearance with the $3p$ distribution showing significantly more off-axis structure than the $3s$ distribution. The origin of this difference can be seen by inspection of the fits in Table II where the $3p$ distribution

TABLE II. Magnesium atomic parameters from nonlinear-least-squares fit to Eq. (12). Standard deviations are indicated in parentheses.

Atomic parameters	$Mg^+(3s)$ 4	$Mg^+(3s)$ 4+1	$Mg^+(3s)$ 4+2	$Mg^+(3p)$ 4+2	$Mg^{2+}(2p^6)$ 7	$Mg^{2+}(2p^6)$ 7+1
	Excitation: 0.532-μm radiation					
β_0	0.90(4)	0.41(3)	0.52(10)	0.77(15)	1.10(27)	0.93(11)
β_2	1.00	1.00	1.00	1.00	1.00	1.00
β_4	1.12(9)	0.77(7)	1.04(25)	0.67(25)	0.64(34)	0.56(16)
β_6	−0.26(6)	0.22(7)	0.69(24)	1.10(31)	0.37(26)	0.90(20)
β_8	0.51(7)	−0.03(7)	0.49(25)	0.58(28)	0.05(39)	0.44(25)
β_{10}		0.11(7)	0.00(25)	0.02(31)	−0.08(42)	0.16(21)
β_{12}			−0.06(25)	0.28(29)	−0.15(47)	0.32(23)
β_{14}					0.38(46)	0.05(25)
β_{16}						−0.07(22)

TABLE III. Magnesium atomic parameters from nonlinear-least-squares fit to Eq. (12). Standard deviations are indicated in parentheses.

Atomic parameters	Excitation: 1.064-μm radiation $Mg^{2+}(2p^6)$ 7	$Mg^{2+}(2p^6)$ 7+1	$Mg^{2+}(2p^6)$ 7+2
β_0	−7.37(77)	−5.12(16)	0.80(10)
β_2	1.00	1.00	1.00
β_4	−4.32(43)	−0.64(39)	0.25(14)
β_6	−2.65(28)	−2.02(83)	0.76(19)
β_8	−1.07(11)	−5.90(105)	1.42(24)
β_{10}	−3.19(12)	3.97(134)	0.88(21)
β_{12}	0.97(14)	−0.55(75)	−0.41(23)
β_{14}	−0.72(11)	−0.45(81)	0.00(24)
β_{16}		−0.38(69)	−0.36(25)
β_{18}			−0.02(24)

has a large contribution from β_6 while the 3s distribution has a large β_4 coefficient, although both have near-zero contributions from higher-L partial waves. The differences in the distributions are not unexpected since an ion left in an excited state will carry some degree of the spatial anisotropy. The angular distributions associated with the 1.28- and 3.6-eV electrons resulting from the sequential ionization of the 3s Mg^+ ground state are also shown in Fig. 4 along with their fits in Table II. The 1.28-eV electron distribution exhibits some degree of broadening which is intensity dependent but independent of the atomic density. This is believed to be a consequence of ponderomotive scattering, whose potential in this distribution is approximately 5–10 % of the field-free electron energy. We were unable to obtain any statistically meaningful distributions below this intensity.

Finally, the photoelectron angular distributions obtained for seven-, eight-, and nine-photon ionization via

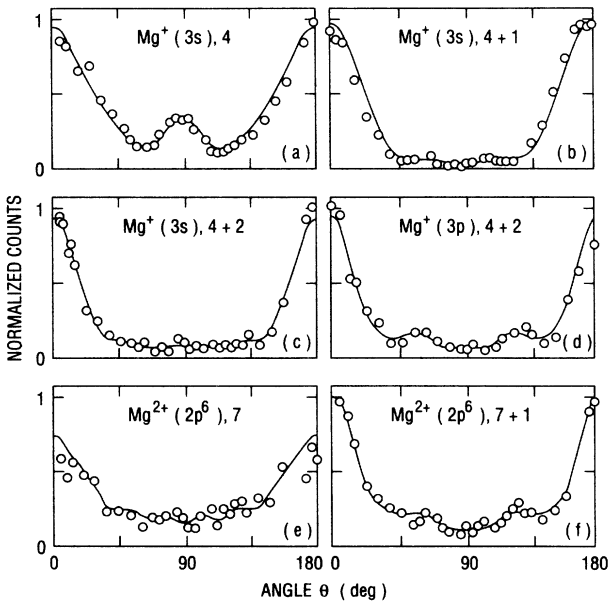

FIG. 4. Electron angular distributions for magnesium with 532-nm excitation. The open circles are the experimental data points and the solid lines are the fit to Eq. (12). The number of photons absorbed are indicated in each plot. The plots are (a) 1.68 eV, $Mg^+(3s)$; (b) 4.01 eV, $Mg^+(3s)$; (c) 6.35 eV, $Mg^+(3s)$; (d) 1.91 eV, $Mg^+(3p)$; (e) 1.28 eV, $Mg^{2+}(2p^6)$; and (f) 3.61 eV, $Mg^{2+}(2p^6)$ channels.

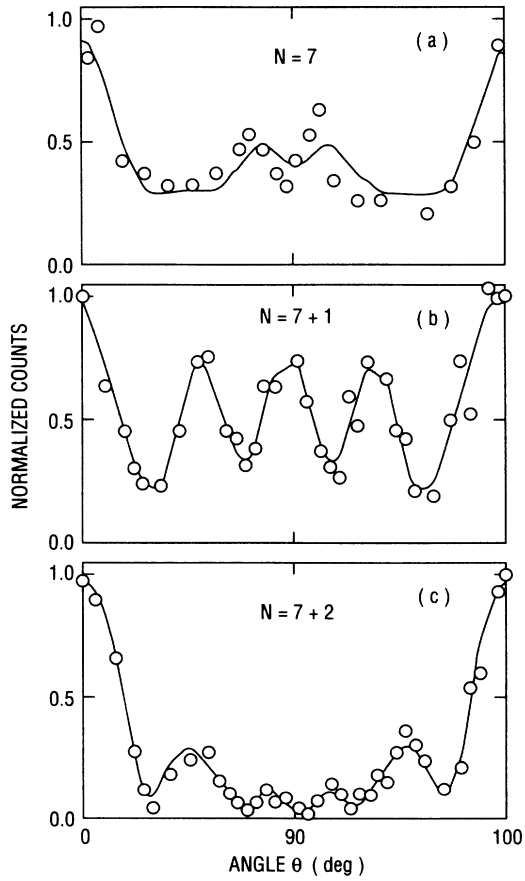

FIG. 5. Electron angular distributions for magnesium with 1.06-μm excitation. The open circles are the experimental data points and the solid lines are the fit to Eq. (12). The number of photons absorbed are indicated in each plot. The plots are (a) 0.51-eV, (b) 1.68-eV, and (c) 2.84-eV $Mg^+(3s)$ channels.

1.06-μm excitation of ground-state Mg atoms are shown in Fig. 5. The β coefficients from the fit to Eq. (12) are listed in Table III. In Fig. 5(a) we again see evidence of ponderomotive scattering of the atomic distribution. The local ponderomotive potential for the lowest-order process corresponds to approximately 70% of the field-free electron energy. However, the distribution in Fig. 5(b) which corresponds to the first ATI peak shows appreciable oscillatory behavior. Systematic errors have been virtually eliminated and reproducibility carefully checked. Scattering, whether field or charge, can be eliminated as the cause, since such mechanisms can only smear and not enhance the photoelectron structure. This distribution is presumably caused by a final-state effect such as autoionization but no states are known in this energy region. However, the fit in Table III shows relatively large values for the β_8 and β_{10} coefficients, that is, high-L final states. No spectroscopy exists for such high angular momentum states. Future plans include scanning this energy region with tunable radiation to gain more insight into the origin of this anomalous distribution.

IV. CONCLUSIONS

Single and double nonresonant ionization of magnesium atoms has been studied over the intensity range of $10^{10}-10^{13}$ W/cm^2 with both 0.532- and 1.06-μm radiation. The results of this study on magnesium demonstrate the important influence that the details of the atomic structure have in describing the nonresonant ionization process. For magnesium, as well as other alkaline earth atoms, the density of atomic states near threshold for both positive and negative energies is high and consequently has an influence on the ionization dynamics. This is further exemplified in the case of magnesium and calcium[14] by the observation that electron correlations via doubly excited states are important for the nonlinear production of singly ionized atoms for both wavelengths studied. This implies that an independent electron model that encompasses more details about the atomic structure than a standard KFR model would still result in an inadequate description of the ionization dynamics. Thus, a more complete calculation must incorporate correlation effects.[17] The dominant mechanism for the production of doubly charged magnesium ions is sequential ionization, although our sensitivity was limited only to electron detection. However, this result invokes a consistent picture with earlier studies on high-Z alkaline earth atoms. The majority of the studies on alkaline-earth atoms have been confined to the long pulse regime. It would be interesting to test whether the above generalizations are valid in the short pulse regime. Such studies would have the consequence of increasing the saturation flux, thus increasing the peak intensities the atom can experience. If doubly excited states continue to play a major role in the ionization dynamics, this could result in an observable production of direct two-electron ionization.

ACKNOWLEDGMENTS

This research was carried out at Brookhaven National Laboratory under Contract No. DE-AC02-76CH00016 with the U.S. Department of Energy and supported, in part, by its Division of Chemical Sciences, Office of Basic Energy Sciences. Partial support was received from the National Science Foundation under Grant No. PHY 88-96134.

---

*Current address: Research Institute of Industrial Science and Technology, Pohang, Kyung buk, Korea.

†Permanent address: Department of Physics, State University of New York at Stony Brook, Stony Brook, NY 11794.

‡Permanent address: Department of Physics, Louisiana State University, Baton Rouge, LA 70803.

[1]P. Agostini, M. Clement, F. Fabre, and G. Petite, J. Phys. B **14**, L491 (1981).

[2]P. Bucksbaum, M. Bashkansky, R. R. Freeman, T. J. McIlrath, and L. F. DiMauro, Phys. Rev. Lett. **56**, 2590 (1986).

[3]P. Kruit, J. Kimman, H. Muller, and M. Van der Wiel, Phys. Rev. A **28**, 248 (1983).

[4]M. Ferray, A. L'Huillier, X. F. Li, L. A. Lompre, G. Mainfray, and C. Manus, J. Phys. B **21**, L31 (1988).

[5]H. R. Reiss, Phys. Rev. A **22**, 1786 (1980).

[6]H. R. Reiss, J. Phys. B **20**, L79 (1987).

[7]M. D. Perry, A. Szoke, O. L. Landen, and E. M. Campbell, Phys. Rev. Lett. **60**, 1270 (1988).

[8]R. R. Freeman, P. H. Bucksbaum, H. Milchberg, S. Darack, D. Schumacher, and M. E. Geusic, Phys. Rev. Lett. **59**, 1092 (1987).

[9]H. G. Muller, H. B. van Linden van den Heuvell, P. Agostini, G. Petite, A. Antonetti, M. Franco, and A. Migus, Phys. Rev. Lett. **60**, 565 (1988).

[10]X. Tang, A. Lyras, and P. Lambropoulos, Phys. Rev. Lett. **63**, 972 (1989).

[11]U. Eichmann, Y. Zhu, and T. F. Gallagher, J. Phys. B **20**, 4461 (1987).

[12]P. Agostini and G. Petite, J. Phys. B **17**, L811 (1984).

[13]D. Feldman, J. Krautwald, S. L. Chin, A. von Hellfeld, and K. H. Welge, J. Phys. B **15**, 1663 (1982).

[14]L. F. DiMauro, Dalwoo Kim, M. W. Courtney, and M. Anselment, Phys. Rev. A **38**, 2338 (1988).

[15]C. H. Greene, Phys. Rev. A **23**, 661 (1981).

[16]K. Codling, L. J. Frasinski, P. Hatherly, and J. R. M. Barr, J. Phys. B **20**, L525 (1987).

[17]X. Tang, T. N. Chang, P. Lambropoulos, S. Fournier, and L. F. DiMauro, Phys. Rev. A (to be published).

[18]C. H. Greene (private communication). An eigenchannel R-matrix method is used to solve variationally the two-electron problem within a finite volume ($r<r_0=14$ a.u.). The two outermost electrons are assumed to move in a screened one-electron potential. The electron motion outside this volume is treated analytically using standard multichannel-quantum-defect-theory techniques. The readers are referred to P. F. O'Mahony and C. H. Greene, Phys. Rev. A **31**, 250 (1985), and C. H. Greene and L. Kim, Phys. Rev. A **36**, 2706 (1987), for details about the methodology.

[19]P. Lambropoulos and X. Tang, J. Opt. Soc. Am. B **4**, 821 (1987).

[20]R. R. Freeman, T. J. McIlrath, P. H. Bucksbaum, and M. Bashkansky, Phys. Rev. Lett. **57**, 3156 (1986).

[21]R. R. Freeman, P. H. Bucksbaum, and T. J. McIlrath, IEEE J. Quantum Electron. **24**, 1461 (1988).

[22]T. J. McIlrath, P. H. Bucksbaum, R. R. Freeman, and M. Bashkansky, Phys. Rev. A **35**, 4611 (1987).